Radial and rotational velocities of young brown dwarfs and very low-mass stars in the Upper Scorpius OB association and the ρ Ophiuchi cloud core

Ryuichi Kurosawa* and Tim J. Harries

School of Physics, University of Exeter, Stocker Road, Exeter EX4 4QL

ABSTRACT

We present the results of a radial velocity (RV) survey of 14 brown dwarfs (BDs) and very low-mass (VLM) stars in the Upper Scorpius OB association (UScoOB) and 3 BD candidates in the ρ Ophiuchi dark cloud core. We obtained high-resolution echelle spectra at VLT using Ultraviolet and Visual Echelle Spectrograph (UVES) at two different epochs for each object, and measured the shifts in their RVs to identify candidates for binary/multiple systems in the sample. The average time separation of the RV measurements is 21.6 d, and our survey is sensitive to the binaries with separation < 0.12 au. We found 2 out of 17 objects (or 12^{+13}_{-10} per cent by fraction) show a significant RV change in 4–33 d time scale, and are considered as binary/multiple 'candidates.' We found no double-lined spectroscopic binaries in our sample, based on the shape of cross-corelation curves. The RV dispersion of the objects in UScoOB is found to be very similar to that of the BD and VLM stars in Chamaeleon I (Cha) previously studies by others. We also found the distribution of the mean rotational velocities ($v \sin i$) of the UScoOB objects is similar to that of the Cha I, but the dispersion of $v \sin i$ is much larger than that of the Cha I objects.

Key words: stars: binaries:spectroscopic – stars: low-mass, brown dwarfs – stars: formation – stars:planetary system: formation

1 INTRODUCTION

Most stars are member of binary systems and it is therefore important that a complete star formation theory be able to predict the binary fraction, period distribution, and mass-ratio distribution of newly born stellar objects across a wide range of masses. Furthermore, the study of the individual binary system is the only direct means to determine the fundamental stellar properties such as stellar masses and radii.

Recent high-resolution imaging studies of young brown dwarfs (BDs) and very low-mass (VLM) stars have placed strong constraints on binaries with separations of $\sim 1 - 100$ au. For example, Hubble Space Telescope (*HST*) observations of α Per and the Pleiades indicates a binary fraction (f) of > 10 per cent with a bias towards separations (a) of less than 15 au, and a mass-ratio (q) of > 0.7 (Martín et al. 2003) for objects around and below the hydrogen burning limit (see also Bouy et al. 2006). A similar lack of wide binaries was found in the field T-dwarf study (Burgasser et al. 2003), while $f = 15$ per cent was determined by Close et al. (2003) using the adaptive optics at Gemini North. They also found an upper limit to the semimajor axis distribution of ~ 20 au. An

HST study of more than 80 field late M and L dwarfs (Gizis et al. 2003) indicated $f = 15$ per cent with separations in the range of 1.6–16 au. For s small sample (12) of BDs and VLM stars (0.04–0.1 $M_\odot$) in Upper Scorpius OB association (UScoOB), Kraus et al. (2005) found $f = 25^{+16}_{-8}$ per cent for $5\,\text{au} < a < 18\,\text{au}$ by using a similar imaging technique. More recently, Basri & Reiners (2006), combined with the results of earlier works, found the upper limit of the overall binary fraction for VLM stars of 26 ± 10 per cent.

Using a Monte Carlo simulation, the data from radial velocity surveys available in the literature, and by carefully considering the sensitivity and sampling biases, Maxted & Jeffries (2005) found an overall BD/VLM binary frequency of 32–45 per cent assuming $f = 15$ per cent for $a > 2.6$ au. A recent photometric study (Pinfield et al. 2003) of low-mass objects in Pleiades and Praesepe suggested, albeit indirectly, f as large as 50 per cent. which would only be compatible with direct imaging studies if 70–80 per cent of those binaries have $a < 1$ au. For a more comprehensive review of the current status of BD/VLM binary fraction and the separation distribution, readers are refer to a recent review of multiplicity studies by Burgasser et al. (2006).

The extensive imaging surveys provide excellent observational constraints on wider BD+BD binaries, but it is now necessary to search for shorter period BD+BD binaries systemati-

---

* E-mail: rk@astro.ex.ac.uk

cally. Binaries with the separation of less than 1 au are not resolved by current imaging techniques, but will be detectable as spectroscopic binaries, providing the mass-ratio is not too extreme, and velocity separation is large enough. The first BD+BD spectroscopic binary, PPl 15 (Basri & Martín 1999) showed a double-peaked cross-correlation function with a maximum velocity separation of $> 70 \, \mathrm{km \, s^{-1}}$. The binary was found to have an eccentric orbit ($e = 0.4$) with a period of $\sim 5.8 \, \mathrm{d}$. Basri & Martín (1999) suggested that the formation process of substellar objects is biased towards smaller separation binaries based on the short period of PPl 15 and the lack of Pleiades BD binaries with separations $> 40 \, \mathrm{au}$. Note that the median separation of binaries with solar-type primaries is 30 au Duquennoy & Mayor (1991). Pioneering work on the RVs of BDs and VLMs are presented by Guenther & Wuchterl (2003), Kenyon et al. (2005) and Joergens (2006b) who found a several binary candidates; however, the orbital parameters and masses of binaries remains unknown because the follow-up spectroscopic monitoring is lacking or still being undertaken. In addition to the follow-up observations, the number of BDs and VLM star binary candidates needs to be increased in order to have better statistics on short-period binary parameters.

The separation distribution of BD/VLM binaries is critical to understanding their origin. There are two main models for the formation of BDs and VLM stars: first, they formed in a similar manner to higher mass stars, but from smaller-mass, denser molecular cloud core (e.g. Padoan & Nordlund 2002); second, BD/VLM objects have low masses because they are ejected from the dense core in which they form via dynamical interactions in multiple system, cutting off their accretion before they have reached stellar masses (Reipurth & Clarke 2001; Bate et al. 2002). Alternatively, there is a third model in which a free-floating BD or planetary-mass object can be formed in the process of the photo-evaporation (Whitworth & Zinnecker 2004) with the outer layers of a pre-stellar core ($\sim 0.2 \, \mathrm{M_\odot}$) removed by the strong radiation pressure from the nearby massive OB stars before the accretion onto the protostar at core centre occurs.

Due to the dynamical interaction involved in the second model, BD/VLM binaries that survive are generally expected to have small separations. In the first model, wider binaries may be expected to be more common. Bate et al. (2002) suggested that close binaries ($a < 10 \, \mathrm{au}$) do not form directly, but result from hardening of wider systems though a combination of dynamical interactions, accretion and interactions with circum-binary discs. If BD/VLM binaries have formed through such mechanisms, one would not expect to find binaries with 1–10 au separations without also finding many with separation $< 1 \, \mathrm{au}$. If an absence/rarity of binaries with 1 au were found, it would support the idea that they are ejected quickly from multiple systems before they have undergone the interactions that shorten their periods.

Our immediate aim is to identify spectroscopic and close BD/VLM binaries using the high-resolution echelle spectroscopy at two epochs. This experiment is sensitive to VLM binaries with separations of $< 0.1 \, \mathrm{au}$ which corresponds to a period of $\sim 10 \, \mathrm{d}$. A larger sample of candidates will enable us to measure the binary fraction of these short-period/close binaries (once confirmed), and address whether there is a significant population of 'hidden' VLM companions. The long term goal of this project to follow up the binary candidates found in this paper by spectroscopically monitoring them over different time scales, enabling us to obtain the radial velocity curves and their minimum masses.

In Section 2. we describe the observations and the data reduction. The results of radial velocity and rotational velocity ($v \sin i$)

measurements are presented in Section 3. We discuss the binary/multiplicity fraction indicated by our RV survey, and compare our results with earlier works in Section 4, and give our conclusions in Section 5.

2   OBSERVATIONS

Our sample consists of 18 young, very low-mass objects: 15 objects in the Upper Scorpius OB association (d $\approx$ 145 pc, de Zeeuw et al. 1999) from the list of Ardila et al. (2000) and 3 objects in the ρ Ophiuchi cloud core (d $\approx$ 150 pc, de Zeeuw et al. 1997) from Luhman & Rieke (1999). The spectral type of the objects range between M5 and M8.5, and the age $<\sim 10 \, \mathrm{Myr}$ (Luhman & Rieke 1999; Ardila et al. 2000; Muzerolle et al. 2003; Kraus et al. 2005). The sample is not complete, and the selection was solely based on brightness and the observability. The basic properties of the targets based on the literature is summarised in Table 1.

We obtained high-resolution spectra with the Kueyen telescope of VLT (Cerro Parnal, Chile) using the UVES echelle spectrograph. The observations were carried out between 2004 April 5 and 2004 May 17 in the service mode. For each object, spectra were obtained at two different epochs separated by 4–33 d. For each object at a given night, two separate spectra are obtained consecutively. This allows us to derive more reliable uncertainty estimates in the RV values of our targets (c.f. Joergens 2006b). The data were obtained using the red arm of UVES spectrograph with two mosaic CCDs (EEV + MIT/LL with 2k×4k pixels). The wavelength coverage of 6708 – 10,250 Å and the spectral resolution $R \approx 40,000$ were used. The slit width and length of 1" and 12" were used respectively with a typical seeing of 0.8".

The data were reduced via the standard ESO pipeline procedures for UVES echelle spectra. In summary, the data were corrected for bias, interorder background, sky background, sky emission lines and cosmic ray hits. They were then flattened, optimally extracted, and finally the different orders were merged. No binning was performed to achieve high resolution required for the RV measurements. The wavelength was calibrated using the Thorium-Argon arc spectra with a typical value of the standard deviation of the dispersion solution of 5 mÅ which corresponds to 0.2 km s^{-1} at the central wavelength 8600 Å. However, the autoguiding of the telescope keeps the star at the centre of the slit with about a tenth of the FWHM (1 km s^{-1}) which sets the upper limit for the systematic error in the RV measurements (Bailer-Jones 2004). The accuracy of the wavelength calibration will be demonstrated in the RV measurements of a RV standard in the following section. A typical signal-to-noise ratio (S/N) per wavelength bin of the spectra is about 15, and the heliocentric velocity correction was applied to the final spectra.

3   RESULTS

3.1   Radial velocities

The radial velocities of each object were determined by using the cross-correlation function of the object spectrum with that of a template star which has a similar spectra type. By visual inspection, the wavelength ranges used for the cross-correlation calculations are chosen by avoiding the regions of spectra affected by the telluric lines, and defects and fringes (in near infrared) of the CCDs. The radial velocities of objects with respect to the template are obtained by measuring the location of the peak in the

Table 1. Summary of known properties of the targets from literatures: a. Luhman & Rieke (1999) (original list for ρ Oph), b. Ardila et al. (2000) (original list for UScoOB), c. Wilking et al. (1999), d. Muzerolle et al. (2003), e. Kraus et al. (2005), and f. Mohanty et al. (2005).

Object	Sp.	mass [M$_\odot$]	RV [km s^{-1}]	$v \sin i$ [km s^{-1}]	Known multiple?
GY 5	M7[c]	0.07[d]	-6.3 ± 1.9[d]	16.8 ± 2.7[d]	no
GY 141	M8.5[a]	0.02[d]	...	6.0[f]	no
GY 310	M8.5[c]	0.08[a,d]	...	10.0[f]	no
USco 40	M5[b]	0.1[b]	...	37.5[f]	no
USco 53	M5[b]	0.1[b]	...	45.0[f]	no
USco 55	M5.5[b]	0.10 + 0.07[e]	...	12.0[f]	yes[e]
USco 66	M6[b]	0.07 + 0.07[e]	-4.4 ± 0.6[d]	27.5[f]	yes[e]
USco 67	M5.5[b]	0.10[e]	...	18.0[f]	no
USco 75	M6[b]	0.07[e]	-5.6 ± 1.1[d]	63.0[f]	no
USco 100	M7[b]	0.05[e]	-8.9 ± 0.6[d]	50.0[f]	no
USco 101	M5[b]	0.05[b]	...	...	no
USco 104	M5[b]	0.05[b]	...	16.0[f]	no
USco 109	M6[b]	0.07 + 0.04[e]	-3.8 ± 0.7[d]	6.0[f]	yes[e]
USco 112	M5.5[b]	0.1[e]	...	8.0[f]	no
USco 121	M6[b]	0.02[b]	-38.9 ± 1.0[d]	...	no
USco 128	M7[b]	0.05[e]	-3.0 ± 1.6[d]	0.0[f]	no
USco 130	M7.5[e]	0.04[e]	...	14.0[f]	no
USco 132	M7[b]	0.05[e]	-8.2 ± 1.1[d]	...	no

cross-correlation function. The location of the peak is determined by fitting the cross-correlation function by a function which consists of two gaussians (with a common centre) plus a constant term. LHS 49 (Proxima Cen, M5.5) was chosen as the template for this purpose. The radial velocity of the template object LHS 49 was obtained by measuring the wavelength shifts of the prominent photospheric absorption features K I $\lambda\lambda$7664.911, 7698.974. This gives us $\mathrm{RV_{LHS49}} = -22.6 \pm 0.5\,\mathrm{km\,s^{-1}}$, which is in good agreement with the earlier measurement of García-Sánchez et al. (2001) who found $\mathrm{RV_{LHS49}} = -21.7 \pm 1.8\,\mathrm{km\,s^{-1}}$. The heliocentric RV of each object can be then calculated by adding $\mathrm{RV_{LHS49}}$ with the RV of each object with respect to LHS 49. In the following measurements of the heliocentric radial velocities, our measurement ($\mathrm{RV_{LHS49}} = -22.6 \pm 0.5\,\mathrm{km\,s^{-1}}$) will be used for consistency.

Before applying the cross-correlation technique to out main targets, we have applied the technique to the radial velocity standard HD 140538 for which an high-accuracy RV measurement via the fixed-configuration, cross-dispersed échelle spectrograph Elodie (Baranne et al. 1996) is available. This was done so to ensure not only the validity of the cross-correlation technique, but also the validity of the wavelength calibration. In this test, we found the heliocentric $\mathrm{RV_{HD\,140538}} = 18.8 \pm 0.6\,\mathrm{km\,s^{-1}}$ which is in good agreement with the Elodie radial velocity measurement of $19.00 \pm 0.05\,\mathrm{km\,s^{-1}}$ (Udry et al. 1999).

The result of the heliocentric RV measurements (from two epochs for each object) is summarised in Table 2 along with the uncertainties. The table also lists the uncertainties in the 'relative' radial velocities (σ_{RRV}) which is the uncertainty of RV with respect to the template star. The two consecutive measurements of RVs (from same nights) are used to find the (absolute/heliocentric) RV of the night, and their uncertainties are obtained from the standard deviations of the mean (σ_{RRV}) and the uncertainty of the template RV value (c.f. Joergens 2006b). Note that for finding a shift in the radial velocities from two different epochs, only σ_{RRV} is important since one only requires relative (with respect to a template) RV values. The 'average' radial velocities ($\overline{\mathrm{RV}}$) of the two epochs

are also given in the same table. The $\overline{\mathrm{RV}}$ values of the objects in UScoOB are consistent with the earlier measurements of Muzerolle et al. (2003) in Table 1.

For each object and for each RV measurement, the deviations (ΔRV) from the average RV are computed and summarized in Fig. 1 along with their uncertainties (σ_{RRV}) in order to aid the identification of multiplicity candidates. Note that in computing ΔRV we do not require the knowledge of absolute or the heliocentric radial velocities, but only the relative velocities (with respect to a template).

To identify an object with a RV variation with a statistical significance from our sample, we apply the method described by Maxted & Jeffries (2005), which we briefly summarize next, to our data. There are three steps in this method: (1) compute the χ^2 by fitting the two-epoch RV data for each object with a constant function (a zero-th order polynomial), (2) compute the corresponding χ^2 probability (p), (3) designate the object as a non-constant RV object or a binary candidate if $p < 10^{-3}$ (1 per cent). When computing χ^2, we use the uncertainties in the relative RV (σ_{RRV}). The number of degree of freedom in the fitting procedure is obviously 1. A similar method was also used in a recent RV survey of VLM stars by Basri & Reiners (2006).

We have computed p for all the objects, and have plotted the results as a histogram of the $-\log p$, shown in Fig. 2 (excluding the non-member USco 121; see explanation later). The figure clearly shows two distinctive populations: one on the left (with small $-\log p$ values) occupied by the RV constant objects, and one on in the right-most bin (with the largest $-\log p$) occupied by the RV variable objects which have $p < 10^{-3}$. The expected distribution of p computed consistently with our uncertainty measurements is also shown in the same figure. The RV constant population on the left side reasonably matches the expected curve. This assures that our uncertainties in RV values are reasonable, and an additional systematic error may not be necessary in this analysis (but see Section 4). According to the figure, there are four objects which show significant RV variations out of 17 samples. They are GY 141, GY 310, USco 55, and USco 104, and considered as our

Table 2. Summary of the observations, the heliocentric radial velocities (RV) from two-epoch and the average rotational velocities ($v \sin i$). The uncertainties of relative radial velocities (σ_{RRV}) with respect to the template star LHS 049 and the average radial velocities ($\overline{\mathrm{RV}}$) are also given.

Object	Date	HJD-2453100	RV $[\mathrm{km\,s^{-1}}]$	σ_{RRV} $[\mathrm{km\,s^{-1}}]$	$\overline{\mathrm{RV}}$ $[\mathrm{km\,s^{-1}}]$	$v \sin i$ $[\mathrm{km\,s^{-1}}]$
GY 5	2004-Apr-24	20.7198440	-6.14 ± 0.84	0.68		
	2004-May-07	33.7721938	-5.96 ± 0.60	0.34	-6.05 ± 1.03	16.5 ± 0.6
GY 141	2004-May-10	36.6712108	-4.39 ± 0.60	0.34		
	2004-May-17	43.6683007	-2.95 ± 0.51	0.11	-3.67 ± 0.79	4.4 ± 1.4
GY 310	2004-Apr-24	20.8373504	-4.83 ± 0.74	0.54		
	2004-May-09	35.8224052	-8.43 ± 0.51	0.11	-6.63 ± 0.90	11.1 ± 6.0
USco 40	2004-Apr-05	1.7661754	-7.15 ± 0.74	0.54		
	2004-May-07	33.7620554	-6.80 ± 0.51	0.11	-6.98 ± 0.90	34.2 ± 0.5
USco 53	2004-Apr-04	0.9036653	-7.27 ± 0.93	1.21		
	2004-May-02	28.7394676	-5.43 ± 0.74	0.55	-6.35 ± 1.19	40.0 ± 0.6
USco 55	2004-Apr-05	1.8422807	-5.39 ± 0.50	0.02		
	2004-May-02	28.8141198	-6.38 ± 0.53	0.27	-6.38 ± 0.73	22.9 ± 0.8
USco 66	2004-Apr-05	1.7972634	-5.32 ± 0.57	0.29		
	2004-May-02	28.7956003	-6.41 ± 0.65	0.42	-5.87 ± 0.86	25.9 ± 1.2
USco 67	2004-Apr-05	1.7188620	-6.01 ± 0.74	0.55		
	2004-May-02	28.7113799	-6.83 ± 0.59	0.31	-6.42 ± 0.90	18.4 ± 0.4
USco 75	2004-Apr-04	0.8840376	-6.75 ± 0.67	0.44		
	2004-May-07	33.6065432	-9.88 ± 1.94	1.88	-8.32 ± 2.05	55.6 ± 3.0
USco 100	2004-Apr-06	1.8179138	-6.76 ± 2.74	2.69		
	2004-May-02	28.7752928	-10.23 ± 1.80	1.73	-8.47 ± 3.28	43.7 ± 3.2
USco 101	2004-Apr-04	0.8120734	-4.22 ± 0.87	0.71		
	2004-May-02	28.6591660	-6.07 ± 0.69	0.48	-5.15 ± 1.11	19.1 ± 0.3
USco 104	2004-Apr-04	0.7850385	-5.83 ± 0.50	0.02		
	2004-May-02	28.6349480	-7.48 ± 0.50	0.06	-6.66 ± 0.06	16.7 ± 0.4
USco 109	2004-Apr-05	1.7453989	-4.15 ± 0.52	0.16		
	2004-May-07	33.6304878	-4.41 ± 0.50	0.03	-5.12 ± 0.72	8.6 ± 1.2
USco 112	2004-Apr-04	0.8552168	-2.70 ± 0.69	0.47		
	2004-May-07	33.5826368	-3.46 ± 0.51	0.11	-3.08 ± 0.86	5.8 ± 1.2
USco 121	2004-Apr-24	20.7059408	-39.47 ± 0.51	0.11		
	2004-May-02	28.6969641	-42.43 ± 0.50	0.02	-40.95 ± 0.71	17.6 ± 1.3
USco 128	2004-May-13	39.7978276	-7.41 ± 0.85	0.69		
	2004-May-17	43.6108024	-6.94 ± 1.16	1.05	-7.18 ± 1.44	3.6 ± 1.1
USco 130	2004-May-09	35.7724090	-4.83 ± 0.54	0.21		
	2004-May-13	39.8538830	-4.95 ± 0.74	0.55	-4.89 ± 0.92	15.2 ± 1.1
USco 132	2004-May-13	39.8268683	-7.18 ± 0.58	0.30		
	2004-May-17	43.6391138	-7.37 ± 1.02	0.89	-7.28 ± 1.17	9.1 ± 0.7

preliminary binary/multiple candidates. We will discuss the effect of the systematics error in detail, and list our final binary/multiple candidate later in Section 4.

Finally, the histogram of $\overline{\mathrm{RV}}$ for the objects in UScoOB is given in Fig. 3. The total number of the objects is 14. Note that USco 121 is excluded from the graph since it is identified as a non-member of the UScoOB association based on the RV value (see Table 2). Muzerolle et al. (2003) also found it to be a likely non-member based on the radial velocity and the low lithium abundance. The distribution of the RVs in the figure was fitted by a gaussian function. We found that the standard deviation and the peak position of the radial velocity distribution are $1.2\,\mathrm{km\,s^{-1}}$ and $-5.9\,\mathrm{km\,s^{-1}}$ respectively. The former is very similar to the standard deviation ($0.9\,\mathrm{km\,s^{-1}}$) of the radial velocity distribution of 9 BDs and VLM objects in Cha I found by Joergens (2006a). They also studied the radial velocity distribution of more massive 25 T Tauri stars in Cha I, and found the standard deviations ($1.3\,\mathrm{km\,s^{-1}}$) is not significantly different from that of the brown dwarfs and the very low-mass objects. Unfortunately, we do not have the radial velocity measurements of the higher mass counter

parts (T Tauri stars) in Upper Sco OB association. This is planned for a near future investigation as this is important for the study of the mass dependency of the kinematics in a young stellar cluster.

According to the hydrodynamical simulations of a low-mass star-forming cluster of Bate et al. (2003) which yields a stellar density of $1.8 \times 10^3\,\mathrm{stars\,pc^{-3}}$, the rms dispersion (1-D) of the stars and the BDs is $1.2\,\mathrm{km\,s^{-1}}$. Similarly for the model with a higher stellar density ($2.6 \times 10^3\,\mathrm{stars\,pc^{-3}}$), the rms dispersion is $2.5\,\mathrm{km\,s^{-1}}$ (Bate 2005). The standard deviation of $\overline{\mathrm{RV}}$ ($1.2\,\mathrm{km\,s^{-1}}$) found in our analysis is more comparable the lower stellar density model.

3.2   Rotational velocities

The rotational velocities of the objects were determined by measuring the widths of the cross correlation functions of the target spectra against a template spectrum from an object which is known to have a very small rotational velocity. The line broadening of the targets is assumed to be dominated by rotational broadening. As in the cases for the radial velocity measurements, LHS 49 is chosen
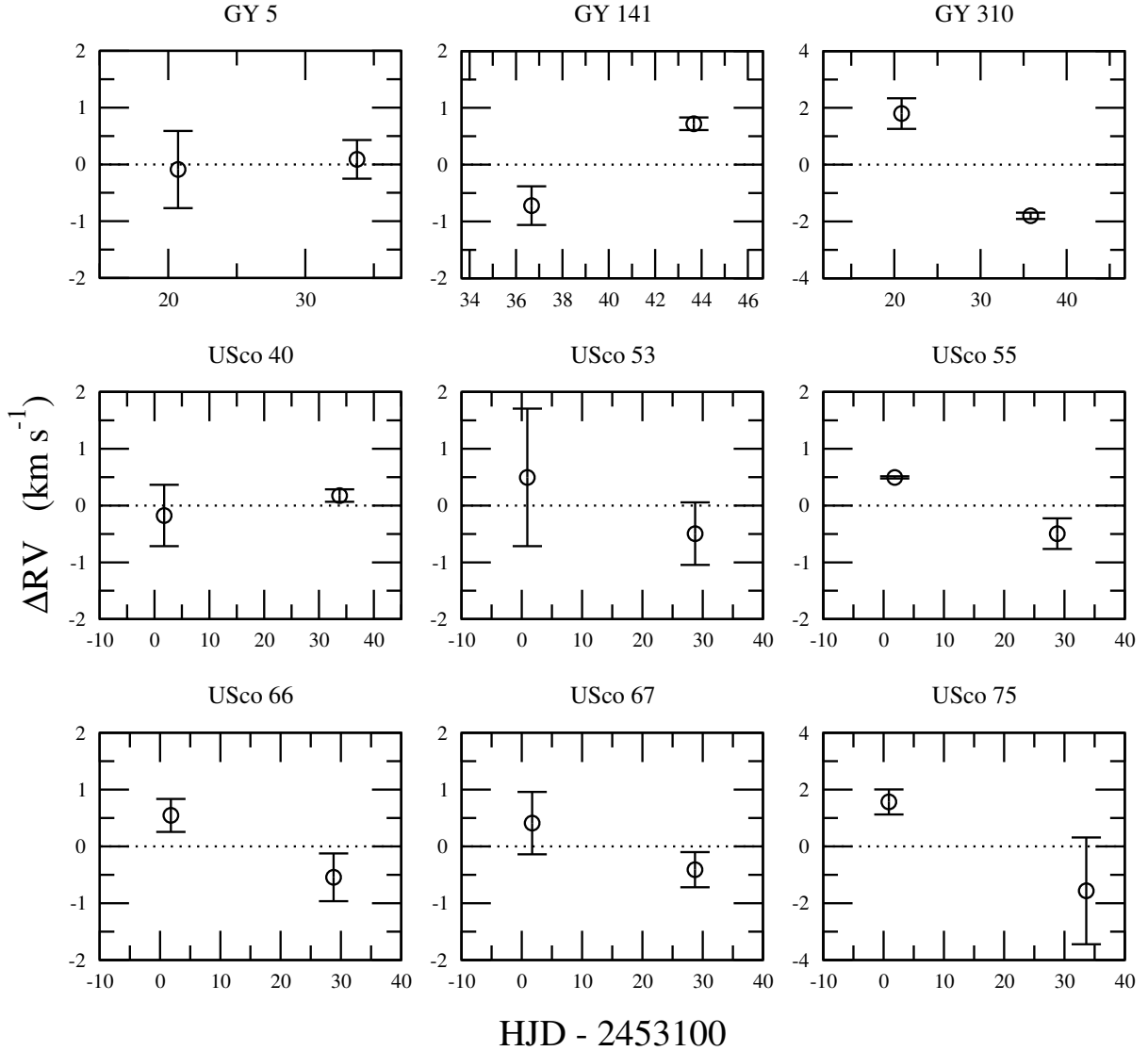
Figure 1. Relative radial velocities (RVs) of objects measured in two different epochs. The vertical axes indicate the amount of deviation (ΔRV) from the 'average' radial velocity ($\overline{\text{RV}}$) in Table 2), and the horizontal axes indicate the time of the observation in heliocentric Julian date (HJD). The objects are considered to have a non-constant RV when the error bars of two data points do not overlap each other. The non-constant RV objects are considered as binary/multiple candidates.

as the template. Using its rotational period ($P \approx 83$ d, Benedict & et al. 1998) and radius ($R_* \approx 0.145$ R$_\odot$ from the VLTI measurement by Ségransan et al. 2003), the rotational velocity of LHS 49 is estimated as $v \sin i = 2\pi R_*/P \approx 0.1$ km s^{-1}; negligibly small.

The width of the cross-correlation curves (σ_{CCF}) are calibrated with the rotational velocities ($v \sin i$) by cross correlating the template spectra against the same template spectra with added rotation (convolved with a given $v \sin i$), as done by e.g. Tinney & Reid (1998), Mohanty & Basri (2003) and White & Basri (2003). A linear limb-darkening law with a solar-like parameter ($\epsilon = 0.6$) was assumed in the formulation of the rotational profile described by Gray (1992), his Eq. 17.12. For each object, two measurements of rotational velocities are computed from two independent spectra obtained at different epochs. As for the RV measurements, the mean and the standard deviation of the mean are used as the final rotational velocity and its uncertainty. The final results are recorded in Table 2. In general, our measurements are in good agreement

with the earlier measurements of Muzerolle et al. (2003) and Mohanty et al. (2005), given in Table 1. For example, Muzerolle et al. (2003) found $v \sin i = 16.8 \pm 2.7$ km s^{-1} for GY 5 while we found $v \sin i = 16.5 \pm 0.6$ km s^{-1}.

The range of $v \sin i$ found among our objects is 3.6–55.6 km s^{-1}, and a similar range is also found by Mohanty et al. (2005). Fig. 4 shows the histogram of $v \sin i$ distribution for the UScoOB objects (14 objects excluding USco 121, non member). The log-normal fit of this distribution gives the peak position at 16.9 km s^{-1} with a standard deviation $\sigma = 27.8$ km s^{-1}. Using the $v \sin i$ data in Joergens & Guenther (2001), the same histogram bin size used for UScoOB obects and the log-normal fit, we find the $v \sin i$ distribution of the BD and VLM stars (8 objects) in Cha I peaks at 15.4 km s^{-1}, and has the standard deviation of 8.0 km s^{-1}. The peak of the distribution is similar to that of Upper Sco objects, but the standard deviation of the distribution is significantly smaller than that of the Upper Sco objects. The difference
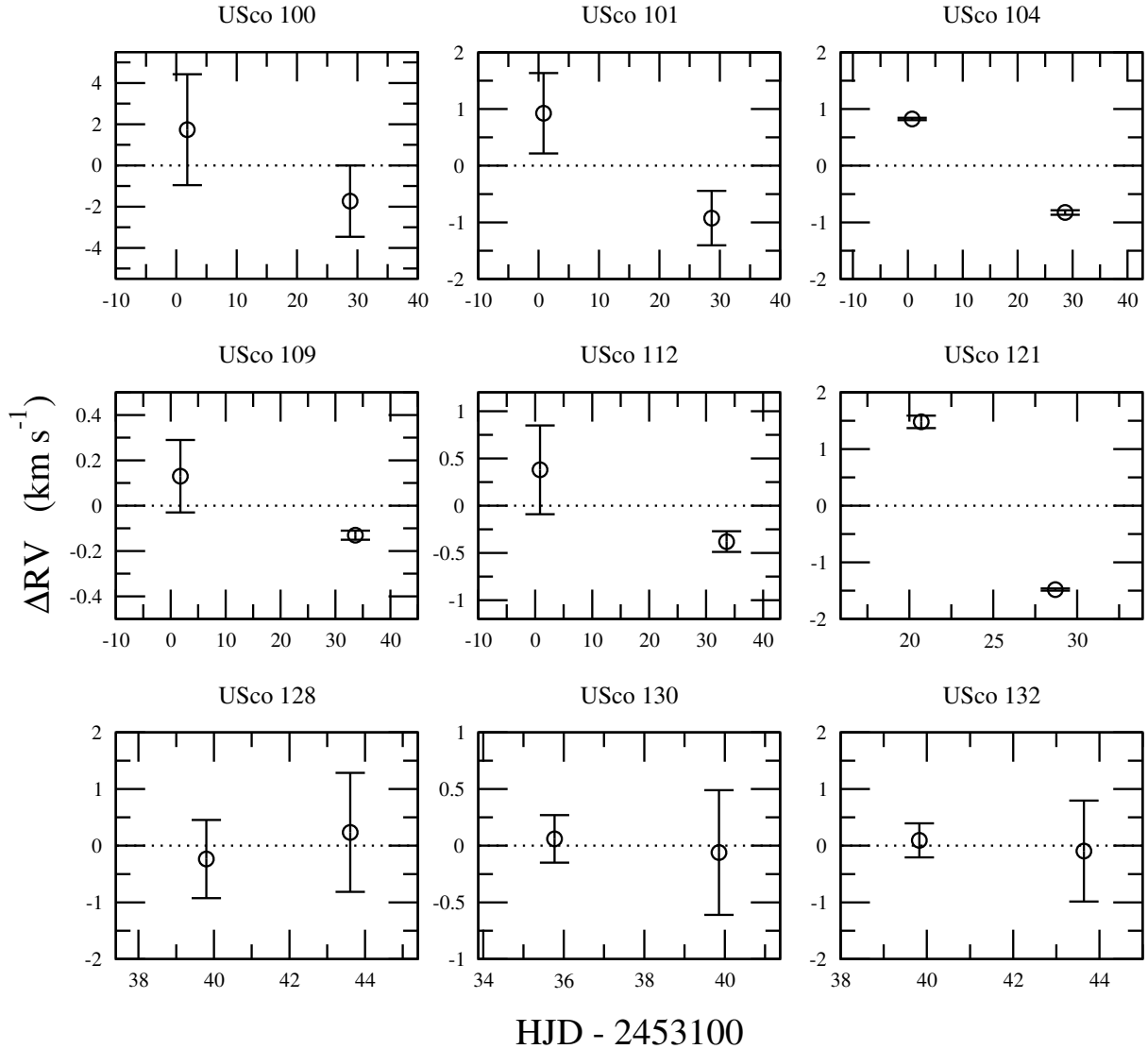
Figure 1. continued

maybe due to the very small sample. A similar fit was applied to the $v \sin i$ distribution of 14 T Tauri stars in Cha I using the data of Joergens & Guenther (2001), and we found a peak at $17.0\,\mathrm{km\,s^{-1}}$ with a standard deviation $25.9\,\mathrm{km\,s^{-1}}$ which are very similar to those of the Upper Sco brown dwarf candidates and VLM stars.

4 BINARY FRACTION

In Section 3.1, we found 4 out of 17 (excluding USco 121; non-member) objects show a statistically significant RV variation, indicating that they are binary/multiple candidates. In order to estimate the uncertainty in the binary/multiple fraction from this relatively small sample, we will follow the method used by Basri & Reiners (2006) who considered the binomial distribution, $P_B(x, n, p)$ of x positive event out of n trials with the probability p for a positive event in each trial. In our case, $n = 17$ (the number sample) and $p = 4/17 = 0.24$ (the fraction of binary/multiple). The uncertainties was estimated by plotting $P_B(x, 17, 0.24)$, and finding the values of x at which P_B reduced to e^{-1} of the peak value. In

this analysis, we find the binary/multiple fraction along with the uncertainties of our sample to be $f = 24^{+16}_{-14}$ per cent.

Next, we investigate the range of semimajor axes of binaries (equivalently the range of binary periods) to which our RV survey is sensitive. For this purpose, we will consider the detection probability for binaries or the RV variables, given the time separations of two-epoch observations and the ranges of estimated primary masses (c.f. Tables 1 and 2). The probability will be calculated based on the simulated RV observations of binaries whose orbit are randomly selected from a model. A similar method was used by Maxted & Jeffries (2005) and Basri & Reiners (2006). The most important factors in determining the detection probability are the size of uncertainties in RV measurements (which we use the average σ_{RRV} from our observation), and the time separations of observations. The smaller the errors in RV measurements, the larger the probability for a given binary orbit and a time separation of orbit. The larger the time separation of observations, the larger the upper limit of the semimajor axis to which an observation is sensitive. The average time separation of the two-epoch RV observations of our targets is 21.6 d. In the following, we will briefly discuss our
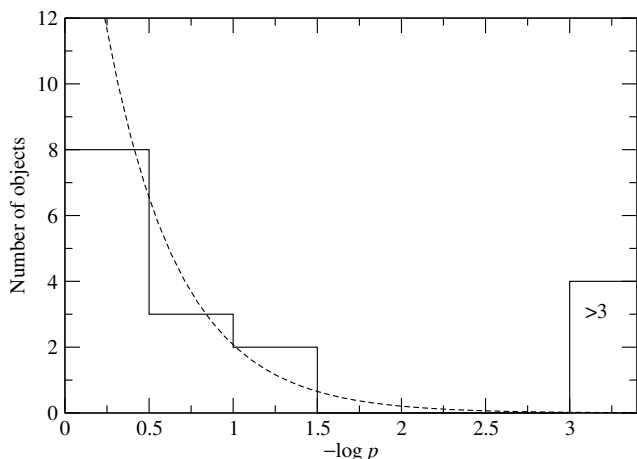
Figure 2. Histogram of the χ^2 probability (p) for fitting the observed (relative) RV values with a constant (a horizontal line). The constant used in the fit is determined from the weighted mean of the two RV measurements for each object. The objects with $p < 10^{-3}$ are identified as *non-constant* or *multiple*, which appear in the right-most bin in the histogram. There are four objects which satisfy this condition. The expected distribution (dashed) for RV constant objects based on the RV uncertainties in the observations (Table 2) and based on the χ^2 probability function is also shown for a comparison. The match between the expected distribution and the histogram is reasonable, indicating that our uncertainty estimates in RV values are also reasonable.
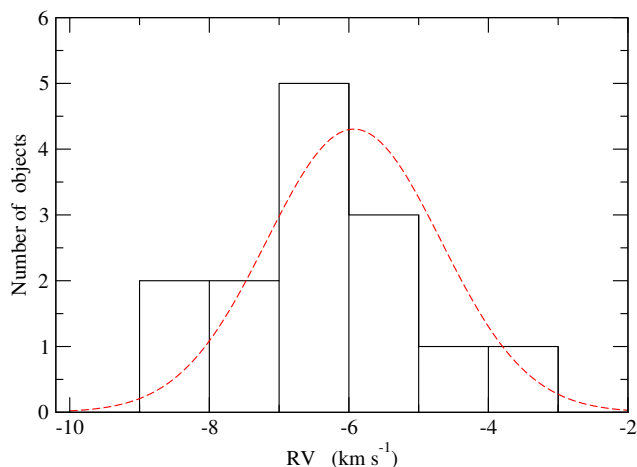
Figure 3. Histogram of the average heliocentric radial velocities of 14 UScoOB BD and VLM objects listed in Table 2 (excluding USco 121, a non-member). The gaussian fit (dashed line) of the radial velociity distribution gives a standard deviation of $1.2\,\mathrm{km\,s^{-1}}$ and the peak position of $-5.9\,\mathrm{km\,s^{-1}}$.

model assumptions and parameters which are essentially the same as those of Maxted & Jeffries (2005) but with some simplifications.

There are six basic parameters our Monte Carlo simulation: primary mass (M_1), mass ratio (q), eccentricity (e), orbital phase (ϕ), orbital inclination (i), longitude of periastron (λ). The primary mass M_1 is assigned from the adopted mass of the targets in Table 1, with a uniform random deviation of $\pm0.002\,M_\odot$. The mass ratio is assumed to be uniformly distributed between $q = 0$ and 0.2. The eccentricity e is assumed to be zero (circular orbits). Both Maxted & Jeffries (2005) and Basri & Reiners (2006) found the
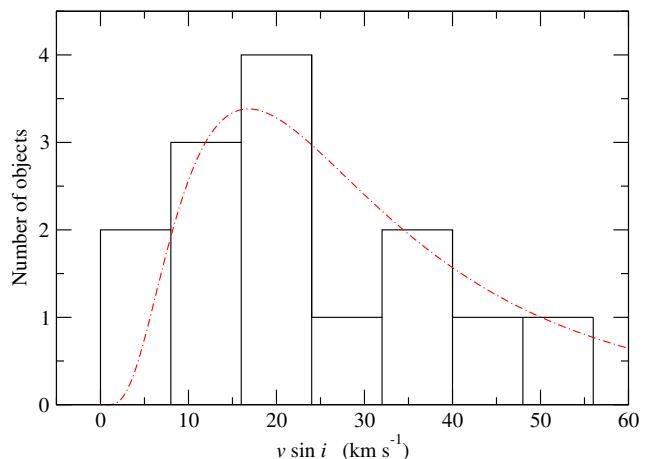

Figure 4. Histogram of the rotational velocities ($v \sin i$) of 14 UScoOB BD and VLM objects listed in Table 2 (excluding USco 121, a non-member). The log-normal fit (dash-dot) of the rotational velocity distribution gives a standard deviation $27.8\,\mathrm{km\,s^{-1}}$ and the peak poistion $16.9\,\mathrm{km\,s^{-1}}$.

detection probability is insensitive to the assumed distribution of q and e. The orbital phase is randomly chosen between 0 and 1. The inclination i is randomly chosen from the cumulative distribution of $\cos i$. The longitude of periastron λ is not necessary since we assumed $e = 0$.

In order to compute the detection probability as a function of semimajor axis a, we take the following procedure: (1) for each object in our targets, we randomly select 10^5 binaries using the assumption stated above for a given value of a, and compute the RV of the primary (V_1), (2) evolve the orbit by the time separation of the RV measurements use in the observations for this object, and take another simulated measurement of RV (V_2), (3) from V_1, V_2 and the average uncertainty in RV (σ_{RRV}) from the observations, we compute the χ^2 probability p, and flag the trial as a detection if $p < 10^{-3}$ as done for the real data, (4) find the fraction of detections out of all random trials, (5) repeat 1–4 for the range of a between 10^{-3} and 10 au, and (6) repeat 5 for the all targets, and find the detection probability averaged over all targets as a function of a.

The result of the simulation is shown in Fig. 5. The detection probability curve shown here is very similar that of Basri & Reiners (2006) for a constant time separation (20 d) case (see their Fig. 4). The probability remains fairly constant up to $a \approx 0.1$ au, and it rapidly decreases beyond $a \approx 0.3$ au. This turning point will increase if we had used larger time separations in our observation. From this figure, we find that the 80 per cent detection probability up to for binaries with $a < 0.12$ au, given our time separations and the average uncertainty ($\sim 0.5\,\mathrm{km\,s^{-1}}$) in the RV measurements.

The expected binary fraction for our survey can be obtained by integrating the product of the detection probability found above with an assumed binary separation distribution function over a range of a. Here, we simply adopt one of the separation distribution function used by Maxted & Jeffries (2005). The binary separation (a) distribution is assumed to be gaussian in $\log(a)$ space with its centre $\log a_o = 0.6$ and width $\sigma_{\log a} = 1.0$, and truncated at $\log a = 1.176$ where a is in au. This form of the distribution function is motivated by the distribution of solar-type binaries found in Duquennoy & Mayor (1991), and the truncation is suggested from the lack of wide binaries for $a > 15$ au (e.g. Burgasser et al. 2003). The distribution is normalized such that the total binary fraction of 26 per cent as suggested by Basri & Reiners
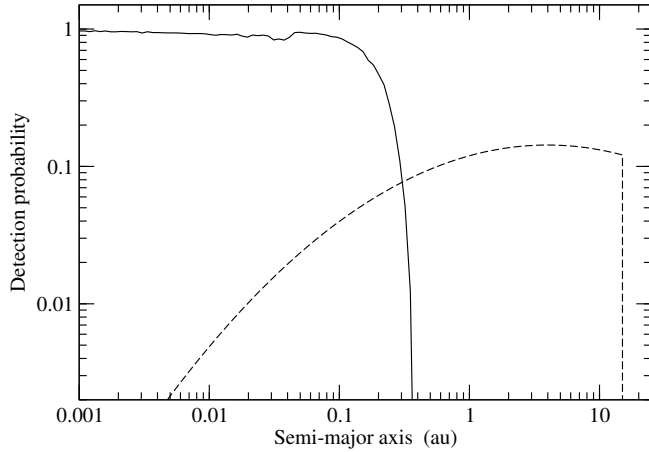
Figure 5. The binary detection probability (solid) as a function of the semi-major axis (a), based on Monte Carlo simulations of RV measurements, is shown. For each object in our target list, the simulation was performed using the time separation (Δt) actually used in our two-epoch observations (c.f. Table 2) and the estimated primary mass (c.f. Table 1). The final detection probability is obtained by averaging over the simulated observations of all the objects. The average time separation in the two-epoch observations is $\sim 21.6\,\mathrm{d}$, and the average uncertainty in RV is $0.5\,\mathrm{km\,s^{-1}}$. The probability remains fairly constant up to $a \approx 0.1\,\mathrm{au}$, and it rapidly decreases beyond $a \approx 0.3\,\mathrm{au}$. The 80 per cent detection probability is achieved for binaries with $a < 0.12\,\mathrm{au}$. The binary separation distribution (dash) similar to that of Maxted & Jeffries (2005) and Basri & Reiners (2006) are shown also for a comparison. The distribution is a gaussinan in logarithmic space, centred at $\log a = 0.6$, and truncated at $a = 15\,\mathrm{au}$. See text for a detail.

(2006). The resulting separation distribution function is shown also in Fig. 5. Using this and the detection probability in the same figure, we find the expected binary fraction to be $f_{\mathrm{exp}} = 3.2$ per cent (for $a < 0.12$ au), which is much smaller than our observed binary fraction of $f_{\mathrm{obs}} = 24^{+16}_{-14}$. The two values are not consistent with each other. There are two possible reasons for the discrepancy: (1) the assumed binary separation distribution mentioned above is unrealistic, and (2) the uncertainties in our RV measurements are underestimated. The first reason is less likely since both Maxted & Jeffries (2005) and Basri & Reiners (2006) found this form of the a distribution function is consistent with the observed binary fractions estimated from many earlier surveys. We will investigate the possibility for the second reason in the following.

Apparently, the underestimated uncertainties could have been caused by neglecting a systematic error. In Section 3.1 (see Fig. 2), we found the histogram of the χ^2 probability p, for the RV data fit assuming constant RV, reasonably matches the expected distribution. This lead us to conclude that the uncertainty estimates in RV values were reasonable. Here, we will inspect the effect of the systematic error on the observed binary fraction more closely. There are two possible source of errors: (1) the RV shifts caused by surface/atmospheric activity, and (2) the RV shifts due to the limit of the stability of autoguiding of the telescope. Joergens (2006b) found that (1) is negligibly small for a young VLM objects with $M_* < 0.12\,M_{\odot}$. The size of RV errors caused by (2) is expected to be $< 1\,\mathrm{km\,s^{-1}}$ (Bailer-Jones 2004). Note that Maxted & Jeffries (2005) found an additional systematic error was not needed to be added to the RV uncertainties of Joergens (2006b) who used the same instruments as ours, and used the same method of estimating
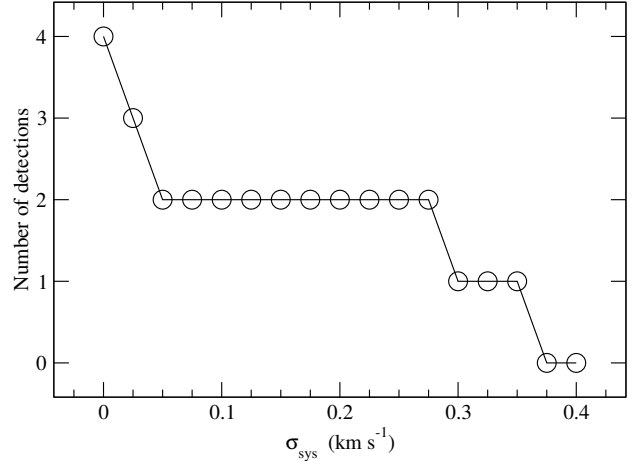
Figure 6. The number of binaries/multiples (non-constant RV objects) detected as a function of the size of additional systematic error (σ_{sys}) in RV measurements. The number of detections decreases rapidly from 4 to 2 as $\sigma_{\mathrm{sys}} = 0.1\,\mathrm{km\,s^{-1}}$, which may be caused by the instability of the autoguiding of the telescope, is added to the uncertainties estimated in Table 2. The number of detections remains constant at 2 for a relatively wide range of the additional errors. i.e. $0.05\,\mathrm{km\,s^{-1}} < \sigma_{\mathrm{sys}} < 0.275\,\mathrm{km\,s^{-1}}$. No binary is found for $\sigma_{\mathrm{sys}} > 0.375\,\mathrm{km\,s^{-1}}$.

the uncertainties. Hence, we expect the systematic error to be much smaller than $< 1\,\mathrm{km\,s^{-1}}$ if one is required.

The observed binary fraction is expected to be very sensitive to the assumed size of the systematic error since the RV shifts and the systematic errors are in same order of magnitude. This point is demonstrated further in Fig. 6 which shows the the number of observed binaries (non-constant RV objects) plotted against the size of the additional systematic error. The number of detections decreases rapidly as σ_{sys} increases. The number remains constant at 2 for a relatively wide range of the systematic errors i.e. $0.05\,\mathrm{km\,s^{-1}} < \sigma_{\mathrm{sys}} < 0.275\,\mathrm{km\,s^{-1}}$. No binary is detected for $\sigma_{\mathrm{sys}} > 0.375\,\mathrm{km\,s^{-1}}$. We have computed the χ^2 probabilities for the RV constant as done earlier (Fig 2) along with the expected distribution of $(-\log p)$ with an additional σ_{sys} introduced in the analysis. We find that the case with $\sigma_{\mathrm{sys}} = 0.1\,\mathrm{km\,s^{-1}}$ gives a better agreement with the histogram of $-\log p$ to the expected distribution (not shown here), compared to the case with $\sigma_{\mathrm{sys}} = 0\,\mathrm{km\,s^{-1}}$. In the following analysis, we will adopt $\sigma_{\mathrm{sys}} = 0.1\,\mathrm{km\,s^{-1}}$. This means that even if our systematic error is slightly underestimated, the number of detection remains the same according to Fig. 6.

We have re-analysed the number of observed binaries (Fig 2), the detection probability (Fig. 5), and the expected binary fraction as done earlier but this time with the additional systematic error $\sigma_{\mathrm{sys}} = 0.1\,\mathrm{km\,s^{-1}}$. The result is summarised in Table 3. Although the small number statistics makes us difficult to withdraw a firm conclusion on the binary fraction from our data, we find the case with $\sigma_{\mathrm{sys}} = 0.1\,\mathrm{km\,s^{-1}}$ has a better agreement with the expected binary fraction (c.f. Table 3). Our tentative conclusion of the binary fraction found in this analysis is $f_{\mathrm{sys}} = 12^{+13}_{-10}$ per cent for $a < 0.12\,\mathrm{au}$. The large uncertainties in this values is due to small number statistics. The expected binary fraction $f_{\mathrm{exp}} = 2.9$ per cent is still within the uncertainty of our binary fraction. The two objects identified as binary/multiple candidates are GY 310 and USco 104.

Table 3. Summary of the observed binary fractions ($f_{\rm obs}$) compared with the expected binary fractions ($f_{\rm exp}$) with and without a systematic error ($\sigma_{\rm sys}$).

$\sigma_{\rm sys}$ (km s^{-1})	N. detected	$f_{\rm obs}$ (per cent)	$f_{\rm exp}$ (per cent)	obj. ID
0.0	4	24^{+16}_{-14}	3.2	GY 141
				GY 310
				USco 55
				USco 104
0.1	2	12^{+13}_{-10}	2.9	GY 310
				USco 104

5 CONCLUSIONS

We have presented two-epoch RV survey of 18 young BDs and VLM stars ($0.02\ M_\odot < M_* < 0.1\ M_\odot$) in UScoOB and ρ Oph dark cloud core using the high resolution UVES echelle spectroscopy at VLT. The average time separation of RV measurements are 21.6 d, and our RV survey is sensitive to binaries with separation smaller than 0.12 au. One of our targets USco 121 is most likely a non-member of the UScoOB association based on the deviation of the RV from the result of the population in the association. A similar conclusion was found by Muzerolle et al. (2003) from their RV study and the low lithium abundance.

We found 2 (GY 310 and USco 104) out of 17 objects as our final binary/multiple candidates. This corresponds to the binary fraction of 12^{+13}_{-10} per cent for the binary separation $a < 0.12$ au, which is larger than the expected binary fraction of 2.9 per cent, but it is still within the uncertainties of the observed value. The expected binary fraction was computed by using a similar binary separation models used by Maxted & Jeffries (2005) and Basri & Reiners (2006). We found that the final estimate of the binary fraction is very sensitive to the assumed size of systematic error. If the systematic error was ignored, we would have found 4 binary/multiple candidates.

The recent high-resolution imaging survey of brown dwarfs and very low-mass objects (M5.5–M7.5) in the UScoOB by Kraus et al. (2005) (which was not known to authors at the time of our observation: April–May, 2004) confirms that USco 65 and USco 66 are multiple systems, and USco 109 is most likely a multiple system. Their projected separations are ($a > 4.0$ au), and are well above our sensitivity limit of 0.12 au. Hence, it is not surprising that we did not find any of them as a multiple, and it also indicates that any of them is unlikely to have a component of a triple system within 0.12 au from their primaries. On the other hand, we found USco 104 as a binary candidate, but this was not in their target list. Further they found USco 67, 75, 112, 128, 130, 132 as non-multiple, and similarly we found them as 'non-candidates' for multiplicity.

We found the RV dispersion ($1.2\,\mathrm{km\,s^{-1}}$) of the objects in UScoOB is very similar to that of the BDs and VLM stars in Chamaeleon I (Cha I) previous study by Joergens (2006a). The rotational velocities ($v \sin i$) of the samples are also measured. The distribution of $v \sin i$ for the UScoOB objects peaks around $16.9\,\mathrm{km\,s^{-1}}$ which is also similar to that of the Cha I population found by Joergens (2006a); however, the dispersion of $v \sin i$ for the UScoOB objects ($27.8\,\mathrm{km\,s^{-1}}$) is found to be much larger than that of the Cha I objects ($8.0\,\mathrm{km\,s^{-1}}$)

The follow-up spectroscopic observations of the binary candidates presented here are planned in near future. There are only a few RV variable binary candidates are identified from the earlier surveys (Guenther & Wuchterl 2003; Kenyon et al. 2005; Joergens 2006b). As Burgasser et al. (2006) pointed out most of the current RV and imaging surveys use samples from magnitude-limited survey, but one should attempt to use the samples from volume-limited survey in order to find a correct statistics on binary parameters more straight forwardly, i.e. without correcting for bias.

References

Ardila D., Martín E., Basri G., 2000, AJ, 120, 479
Bailer-Jones C. A. L., 2004, A&A, 419, 703
Baranne A., Queloz D., Mayor M., Adrianzyk G., Knispel G., Kohler D., Lacroix D., Meunier J.-P., Rimbaud G., Vin A., 1996, A&AS, 119, 373
Basri G., Martín E. L., 1999, AJ, 118, 2460
Basri G., Reiners A., 2006, ArXiv Astrophysics e-prints
Bate M. R., 2005, MNRAS, 363, 363
Bate M. R., Bonnell I. A., Bromm V., 2002, MNRAS, 332, L65
—, 2003, MNRAS, 339, 577
Benedict G. F., et al., 1998, AJ, 116, 429
Bouy H., Moraux E., Bouvier J., Brandner W., Martín E. L., Allard F., Baraffe I., Fernández M., 2006, ApJ, 637, 1056
Burgasser A. J., McElwain M. W., Kirkpatrick J. D., 2003, AJ, 126, 2487
Burgasser A. J., Reid I. N., Siegler N., Close L., Allen P., Lowrance P., Gizis J., 2006, ArXiv Astrophysics e-prints
Close L. M., Siegler N., Freed M., Biller B., 2003, ApJ, 587, 407
de Zeeuw P. T., Brown A. G. A., de Bruijne J. H. J., Hoogerwerf R., Lub J., Le Poole R. S., Blaauw A., 1997, in ESA SP-402: Hipparcos - Venice '97, pp. 495–500
de Zeeuw P. T., Hoogerwerf R., de Bruijne J. H. J., Brown A. G. A., Blaauw A., 1999, AJ, 117, 354
Duquennoy A., Mayor M., 1991, A&A, 248, 485
García-Sánchez J., Weissman P. R., Preston R. A., Jones D. L., Lestrade J.-F., Latham D. W., Stefanik R. P., Paredes J. M., 2001, A&A, 379, 634
Gizis J. E., Reid I. N., Knapp G. R., Liebert J., Kirkpatrick J. D., Koerner D. W., Burgasser A. J., 2003, AJ, 125, 3302
Gray D. F., 1992, The Observation and Analysis of Stellar Photospheres. Cambridge Univ. Press, Cambridge, UK
Guenther E. W., Wuchterl G., 2003, A&A, 401, 677
Joergens V., 2006a, A&A, 448, 655
—, 2006b, A&A, 446, 1165
Joergens V., Guenther E., 2001, A&A, 379, L9
Kenyon M. J., Jeffries R. D., Naylor T., Oliveira J. M., Maxted P. F. L., 2005, MNRAS, 356, 89
Kraus A. L., White R. J., Hillenbrand L. A., 2005, ApJ, 633, 452
Luhman K. L., Rieke G. H., 1999, ApJ, 525, 440
Martín E. L., Barrado y Navascués D., Baraffe I., Bouy H., Dahm S., 2003, ApJ, 594, 525
Maxted P. F. L., Jeffries R. D., 2005, MNRAS, 362, L45

Mohanty S., Basri G., 2003, in The Future of Cool-Star Astrophysics: 12th Cambridge Workshop on Cool Stars, Stellar Systems, and the Sun (2001 July 30 - August 3), eds. A. Brown, G.M. Harper, and T.R. Ayres, (University of Colorado), 2003, p. 683-688., Brown A., Harper G. M., Ayres T. R., eds., pp. 683–688

Mohanty S., Jayawardhana R., Basri G., 2005, ApJ, 626, 498

Muzerolle J., Hillenbrand L., Calvet N., Briceño C., Hartmann L., 2003, ApJ, 592, 266

Padoan P., Nordlund Å., 2002, ApJ, 576, 870

Pinfield D. J., Dobbie P. D., Jameson R. F., Steele I. A., Jones H. R. A., Katsiyannis A. C., 2003, MNRAS, 342, 1241

Reipurth B., Clarke C., 2001, AJ, 122, 432

Ségransan D., Kervella P., Forveille T., Queloz D., 2003, A&A, 397, L5

Tinney C. G., Reid I. N., 1998, MNRAS, 301, 1031

Udry S., Mayor M., Queloz D., 1999, in ASP Conf. Ser. 185: IAU Colloq. 170: Precise Stellar Radial Velocities, Hearnshaw J. B., Scarfe C. D., eds., p. 367

White R. J., Basri G., 2003, ApJ, 582, 1109

Whitworth A. P., Zinnecker H., 2004, A&A, 427, 299

Wilking B. A., Greene T. P., Meyer M. R., 1999, AJ, 117, 469